The response of mild steel and armour steel plates to localised air-blast loading-comparison of numerical modelling techniques

Manuscript

N. Mehreganian[a], L.A. Louca[a], *G.S. Langdon[b], R. J. Curry[b], N.Abdul-Karim[b,c]

[a] *Department of Civil & Environmental Engineering, Imperial College, London, UK*

[b] *Blast Impact and Survivability Research Unit, Department of Mechanical Engineering, University of Cape Town, South Africa.*

[c] *Cranfield Forensic Institute, Cranfield University, Cranfield, UK*

Abstract

This paper presents a comparative study of numerical, experimental and empirical techniques on the effect of localised air blast loads on mild steel and armour steel plates. The blast load effects on monolithic plates have been accounted for by using different approaches provided in the Finite Element hydrocode ABAQUS 6.13, namely an Eulerian Lagrangian and a Coupled Eulerian Lagrangian model. In the first model, the air and the explosive were modelled using multi-material Eulerian grids while the plate was modelled using a rigid Lagrangian mesh, while in the second model the rigid target was replaced with deformable plate.

The transient deformation of the plate, strain localisation, pressure distribution on the plate have been investigated in the FE models, which have been validated against small scale experimental data for a limited range of charge sizes for both the mild steel and armoured steel. Despite the lower deflection of armour steel compared to mild steel plates, both plates were shown to undergo rupture upon similar charge mass and stand-off. For this purpose, a non-dimensional analysis was carried out with consideration of stand-off distance and slenderness ratio to predict the rupture impulse.

Keywords: Blast Loading, numerical techniques, transient response, steel, permanent deflection

1 Introduction

Events such as 9/11 and the recent European bombings (2015-2017) have caused public awareness of explosive threats to increase dramatically. In response to the risk of explosions, efforts have been made to improve the response of civil structures and transportation vehicles to air-blast loading. It is important to understand the loading arising from an explosive detonation and the resulting damage sustained by nearby structures. Careful materials selection can greatly assist in providing much needed blast protection for vulnerable structures, with high strength armour steels (which have been excellent in ballistic applications) being an obvious potential candidate. Such steels provide much higher strengths and hardness (which are good for resisting projectile penetration) but at the expense of reduced ductility [1]–[3].

A blast wave is generated by a rapid release of energy which propagates through a medium. Whether the type of blast is localised, for example, buried land mines, or globalised (far field explosions), the structure may respond in different ways: either deflecting some of the blast wave, or undergoing large inelastic deformation, partial or complete tearing and shear failure. Subject to uniform pressure load, the plate elements may respond in different local modes of failure. The failure modes were initially classified by Menkes and Opat [4] for beams but later developed by Nurick and Radford [5], and Olson et al [6] for plates. These comprised of Mode I-large inelastic deformation, Mode II-large inelastic deformation with tensile tearing at supports and Mode III-transverse shear failure at supports. Jacob et al [7] report similar observations for locally blast loaded plates which included the large inelastic displacement at the centre (mode I), partial tearing at central area (IIc*) and capping or complete tearing at centre (IIc). The locally loaded plate profile is governed by a smaller dome atop a larger dome.

Nomenclature

Latin Upper case

A_0	burn area, [L^2]
B	plate breadth, [L]
C_p	ideal gas specific heat at constant pressure, [$L^2T^{-2}K^{-1}$]
C_v	ideal gas specific heat at constant volume, [$L^2T^{-2}K^{-1}$]
D_e	load diameter [L]
H	thickness of the plate, [L]
I^*	non-dimensional impulse [1]
Î	impulse density, [$ML^{-1}T^{-1}$]
L	plate length, [L]
M_0	maximum moment per unit length, [MLT^{-2}]
S_D	stand-off distance, [L]
R_b	burn radius, [L]
V_0	initial impulsive velocity, [LT^{-1}]
W	plate maximum displacement at centre, [L]
Z	Hopkinson's scaled distance, [LM^{-1}]

Latin Lower Case

a	explosive constant [1]
b	explosive decay constant, [L^{-1}]
m	mass of explosive [M]
r_e	radius of disk explosive, [L]
h_e	charge height, [L]
p_0	maximum explosive pressure, [$ML^{-1}T^{-2}$]
$\dot{w}$	plate velocity, [LT^{-1}]
p_c	static plastic collapse pressure, [$ML^{-1}T^{-2}$]

Greek Lower case

δ, w_f	plate permanent deflection, [L]
$\hat{\theta}$	homologous temperature, [K]
$\dot{\varepsilon}$	material strain rate, [T^{-1}]
ρ	material density, [ML^{-3}]
τ	positive duration of the blast load, [T]
μ_0	dynamic viscosity, [$ML^{-1}T^{-1}$]
μ	areal density, [ML^{-2}]
γ	plate width/length ratio, [1]
$\emptyset_{ql}$	modified normalised(dimensionless) impulse, [1]
$\emptyset_{sl}, \emptyset_{sl'}$	modified normalised impulse with stand -off effects [1]
σ_0	material static yield stress, [$ML^{-1}T^{-2}$]
σ'_y	material dynamic yield stress, [$ML^{-1}T^{-2}$]
σ_{UT}	ultimate tensile stress, [$ML^{-1}T^{-2}$]
λ	dimensionless kinetic energy, [1]
γ'_s , γ_{SL}	dimensionless load parameters, [1]
ω	natural frequency of vibration [T^{-1}]

Nurick et al [8]–[15] have reported considerable experimental data on the response of steel plates to air-blast loading during the past 25 years. Spatial loading distribution (localised versus uniform), explosive mass and shape, boundary conditions, plate size and shape and plate thickness were varied. A non-dimensional impulse parameter, originally proposed in 1989 [10] and subsequently modified [16] to incorporate changes to loading conditions and plate geometries, has been used to collapse the data to a single trend-line which allowed for the prediction of permanent mid-point displacement [9]. A recent review paper by Chung Kim Yuen et al [8] reviewed the abundance of mild steel test data and fitted it all to one trend-line, confirming the trends predicted by Nurick and Martin in 1989 [10].

Neuberger et al [17], [18] conducted experimental studies on the Rolled Homogeneous Armour (RHA) steel subject to air blast and buried charge loading from spherical TNT charges. The deformation combs such as used by Neuberger [18] provides information about the maximum transient displacement of a plate (usually at the mid-point) but cannot give details regarding the time to peak of the deformation profile across the plate. There is also the

possibility of contact measurement techniques influencing the response of the plates, a drawback that can be overcome by using non-contact measurement techniques such as high speed imaging.

Fourney et al [19] and Spranghers et al [20] used high speed photography and 3D Digital Image Correlation (DIC) to measure the transient response of plates subjected to low charge mass explosive detonations. Small apertures on the lenses were used by Spranghers et al [20] to ensure sufficient depth of field for tracking the plate motion, and challenges of changing light conditions on the specimen as it moved. Aune et al [21] used high speed photography to film the motion of a blast loaded plate mounted in a stationary rigid clamp frame. The cameras were placed in the same room at the blast event and Aune et al [21] reported that the blast wave reduced the accuracy of data capture after the blast wave had impinged on the cameras. However, in a later numerical study, Aune et al [22] concluded that the DIC technique was capable of capturing the deflection histories throughout the entire test as long as the movement of the mounting frame was accounted for in the calculations.

Much of the past work on blast loaded plates has concentrated on relatively ductile steels, which exhibit large plastic deformations and then ductile tensile tearing at high charge masses. More recently, there has been interest in high strength steels, such as the ARMOX armour steels. Langdon et al [1] reported the results of localised blast tests on mild steel, ARMOX 370T, aluminium alloy and fibre reinforced polymer composite plates. Permanent mid-point displacement increased linearly with increasing impulse for each material type, up to rupture. At higher charge masses, the mild steel plates exhibited ductile tensile rupture, while the armour steel plates (which ruptured at the same impulse) exhibited a more brittle type of failure. Non-dimensional impulse at rupture was observed to increase with increasing specific energy to tensile fracture (which was obtained by directly integrating the stress-strain curve obtained from uniaxial quasi-static tensile tests) [1].

Measuring the transient deformation history of plates (prior to failure) provides valuable information that improves our understanding of the mechanisms which influence and control the deformation and rupture of plates. This is particularly useful in high strength armour steels where the elastic energy stored during deformation is relatively high, as a proportion of the total deformation energy, compared to mild steel. On the other hand, armour steels have limited ductility compared to mild steel plates which dissipate energy in plastic strain.

Early work on the Fluid Structure Interaction (FSI) by Taylor [23] showed that as the limiting case of a plate with infinite mass is approached, the plate hardly moves and all of the incident pressure is reflected off the plate. Consequently, the impulse imparted to the plate reaches its maximum. In the case of thin plates, however, the plate equilibrates quickly and accelerates which relieves the reflected pressure, thus reducing the impulse. The theoretical work on the FSI effects by Taylor was extended to account for the fluid nonlinear compressibility effects which evaluated the transmitted impulse in terms of a single dimensionless parameter [24], [25].

Advancements in numerical simulations have made it possible to observe the blast wave effects and its interactions with structures, using a Multi Material Eulerian approach. This approach incorporates the governing physics of FSI and was studied by [3], [26]–[28]. Reference [27] observed a significant difference between the transient profiles of box containers due to the difference in the numerical techniques when modelling the pressure time history, despite the same total impulse.

With this rationale, this paper seeks to compare various ways of modelling the blast loading and response of high strength steel plates using the commercially available modelling package ABAQUS/Explicit. A new series of experiments supplements the data reported by Langdon et al [1] on blast response of armour steels. Both sets of data are used to assist with model validation and comparing the various modelling approaches. Given the high strength steels

have considerably higher yield stresses than ductile mild steels, the transient response is considered to be of great importance.

As such, following the introduction, the material models and configurations of test specimen are described in Section 2 and a description of physical experiments presented in Section 03. Section 4 discusses the methodology for numerical models. The validation and comparison of numerical methods are made in section 5, followed by correlating the parameters by dimensionless empirical models. Based on the comparative study, a method for threshold of impulse is proposed for design purposes. In section 6 the conclusions of this study are presented.

2 Model configurations

2.1 Material properties

2.1.1 Constitutive models

With respect to material behaviour, steel shows elastic-plastic behaviour with the associated hardening effects beyond the yield strength. Beyond the ultimate tensile strength, ductile damage-necking and then tearing of the material will occur. The Cowper-Symonds constitutive model by is commonly employed in theoretical as well as the numerical models in the literature[14]–[17], [20], [29], [30]. This equation defines dynamic plastic stress as a function of static yield stress and strain rate as in Eq. (1):

$$\sigma'_y = \sigma_0 \left(1 + \left(\frac{\dot{\varepsilon}}{D} \right)^{1/q} \right) \quad \textbf{(1)}$$

where σ'_y and σ_0 are the dynamic flow stress and static yield stress, respectively, and $\dot{\varepsilon}$ is the uniaxial strain rate. Eq. (1) requires that the strain hardening be known (through uniaxial static tests). The commonly used constants D and q for mild steel are 40.4 (s^{-1}) and 5 [6]. The Cowper Symonds model is phenomenological and tend to give satisfactory results at low strain rates (the range in which they are usually characterised). At high strain rates, the flow stresses increase rapidly and viscous drag controls the dislocation movement. Rolled Homogenous

Armour steel and ARMOX steels are less dependent on the strain rate, for which the parameter $D = 300\ (s^{-1})$ is proposed [17].

Johnson & Cook [31] proposed an alternative model shown in Eq. (2), which takes into account the work hardening effect. The Johnson Cook (JC) model is a multiplicative model, where the work hardening increases with an increase in strain rate. The model estimates the dynamic stress for the strain hardening materials and strain rate effects together with thermal softening.

$$\sigma'_y = [A_1 + B_1\varepsilon^n][1 + Cln\dot{\varepsilon}^*][1 - \hat{\theta}^m] \quad \textbf{(2)}$$

$$\hat{\theta} = \left[\frac{T-300}{T_{melt}-300}\right] \quad \textbf{(3)}$$

where A_1 is the quasi static yield stress, B_1 and n are the hardening constant and exponent, respectively, $\dot{\varepsilon}^* = \dot{\varepsilon}/\dot{\varepsilon}_0$ is the dimensionless plastic strain and $\dot{\varepsilon}_0$ is the reference strain rate, taken as $1s^{-1}$. The homologous temperature, $\hat{\theta}$ can be found from Eq. (3), where T is the temperature in Kelvin and T_{melt} is the melting temperature of the material, taken as 1800K. The Johnson Cook parameters for Armour steel were obtained by the same method discussed by [32]. The results of some models were compared with the Cowper Symonds material plasticity model.

Based on the uniaxial quasi-static test results conducted at Imperial College and stress strain data provided by [1], the average percentage elongation to rupture of ARMOX 440T is 6% and those of ARMOX 370T and Mild steel are 8% and 50%. The Young modulus of all these panels was taken as 207GPa and the Poisson ratio $\upsilon = 0.3$. The yield strength of the panels is represented in Table 1 and a plot of engineering stress vs engineering strain can be seen in Fig. 1 for ARMOX 440T. To obtain the JC parameters for armour steel, the quasi-static tensile test data from [1] was adjusted to the line of best fit shown in Fig. 2. The parameters are summarised in Table 2.

For the purpose of the numerical studies, the predicted true stress and strain curves of ARMOX 370T and Mild steel are calculated from the engineering stress strain curves provided by Ref. [1], [33]. Fig. 3 compares the ultimate true stress of armour 440T calculated numerically (JC model) and experimentally at different strain rates, while a plot of quasi- static strain hardening characteristics is presented in Fig. 4. The specific heat capacity of the steel panels was assumed as $452KJ/kgK$. Due to the instantaneous collision between the blast and the target plate, the heat generated by the plastic flow has no time to transfer and may be assumed as adiabatic. The inelastic heating fraction (Taylor-Quinney coefficient) was taken as 0.9.

Table 1- Material properties of armour steel and mild steel

Plate	Thickness (mm)	σ_0 (MPa)	σ_{UT} (MPa)
ARMOX 370T	3.8	1150	1250
ARMOX 440T	4.6	1210	1400
Mild Steel	4	330	400

Table 2- JC and Cowper Symonds (C.S) material parameters

Material	Johnson Cook					C.S	
	A (MPa)	B (MPa	C	n	m	D	q
ARMOX 370T	1157	837.92	0.015	0.283	0.897	300	5
ARMOX 440 T	1210						
Mild Steel	325	275	0.076	0.36	1	40.4	5

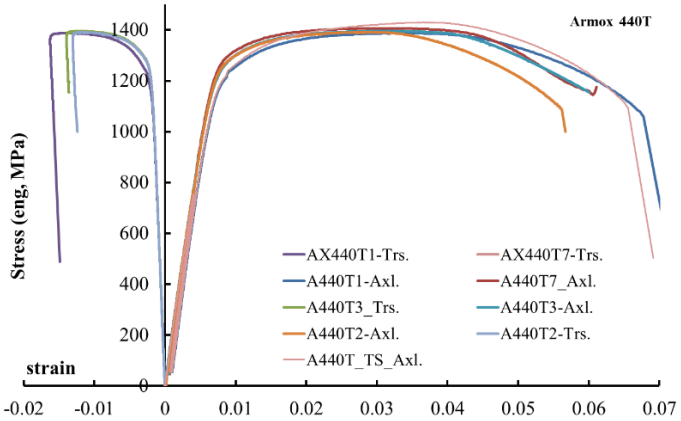

Fig. 1 Quasi-static plot of axial (Axl and transverse (Trs) engineering stress curves for ARMOX 440T, compared against the true stress (TS) curves (For interpretation of colour in this figure, the reader is referred to the online version)

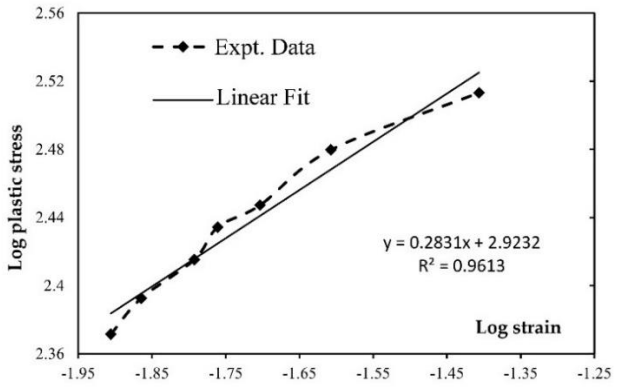

Fig. 2 Log plastic strain vs log plastic stress curve. Notes: The values of B and n are the $10^{(y\ intercept)}$ and the slope of the log (plastic stress) vs log (plastic strain) plot. Constant C is found from the plot of high strain rate sensitivity vs dynamic stress plots [32]. All materials were assumed to have the melting temp and transition temp of 1800K and 293K, respectively

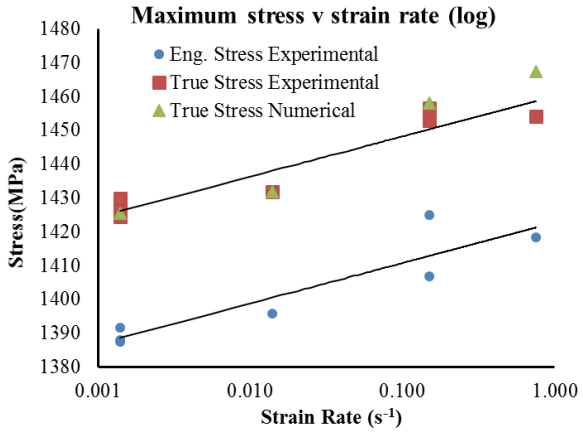

Fig. 3 log plot of the ultimate tensile strength of ARMOX440T at various strain rates

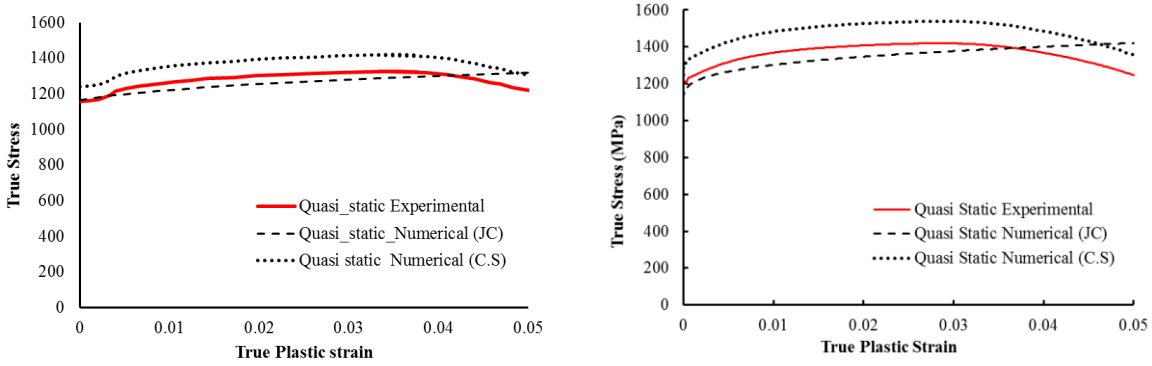

(a) (b)

Fig. 4 Quasi-static strain hardening ($8\times10^{-4}s^{-1}$)-Numerical fit vs experimental data for armour 370T (a) and armour 440T (b). The temperature effects from JC model have been disregarded

3 Description of physical experiments

3.1 Blast test Specimen

Several panels were tested in a specially built blast facility at the Department of Mechanical Engineering at the University of Cape Town shown in Fig. 5. The test plates were made from two high strength steels with the properties shown in Table 1. Each test plate was bolted into the clamps with 12 evenly spaced bolts. The plates were clamped along the periphery between two square clamp frames, leaving a square exposed area of 400 ×400 mm and areal density of 31kg/m^2. The ARMOX440T panels had a higher mass with average nominal thickness of 4.6

mm and areal density of 37kg/m^2. As a comparison, mild steel panels with same dimensions were also tested.

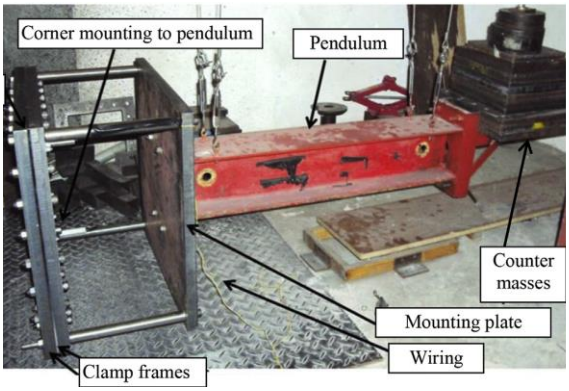

Fig. 5 Experimental test arrangement with horizontal pendulum. Courtesy of [1]**.**

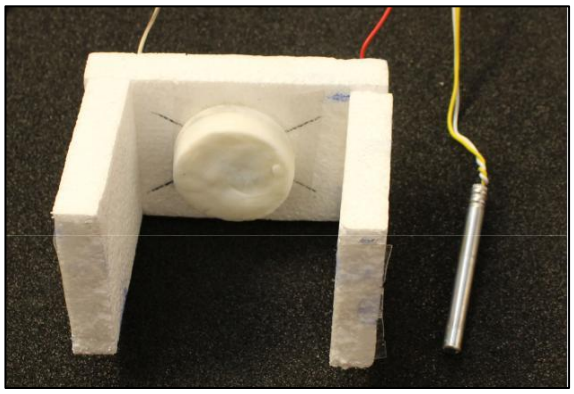

Fig. 6- Photograph of the loading arrangement

Fig. 7- Photograph showing the inside of the modified, DIC pendulum, set up for filming the rear surface of the plates

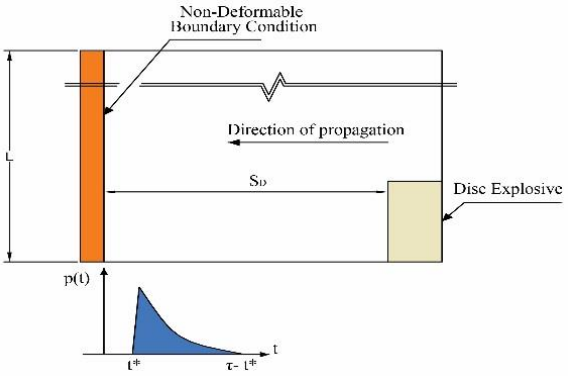

Fig. 8- Eulerian arrangement to gauge the pressure-time history, t^* is the arrival time of the explosive product at the target plate

The clamp frames were mounted to a ballistic pendulum shown in Fig. 5 which measured the impulse imparted on a test plate. Air-blast loading was generated by detonating circular disks of PE4 plastic explosive at a predetermined stand-off distance using M2A3 instantaneous electrical detonators. The PE4 disks were located at the centre of the test plates using a polystyrene bridge arrangement, as shown in Fig. 6. Stand-off distances of 25 mm, 38 mm and 50mm were used, as presented in Table 3, and were set by varying the lengths of the bridge legs. The charge mass was varied by changing the height of the explosive, and ranged from 24g to 70g. Only MSP1 and MSP2 specimens had the charge diameter of 75mm, whereas the charge diameter for the mild steel tests and armour steel was 50mm, except for ASP7 and ASP8

panels which had charge diameters of 40mm. Further details of the test arrangement are discussed in Ref. [34].

A small number (5) of the test plates were tested on the modified pendulum system described by Curry and Langdon [35] which incorporates high speed Digital Image Correlation (DIC) for transient displacement measurements shown in Fig. 7. The new pendulum provided protection for the cameras from the intense light burst and the ensuing blast wave. Two IDT vision NR4 S3 high speed cameras were mounted to a vibration isolated aluminium rail system to prevent independent movement during the testing. The two cameras were oriented to face the rear of the test plate and separated by an approximate 30^o included angle. The synchronised images from the two cameras were triggered with a custom built TTL trigger circuit that was activated by the detonation. A full width strip along the mid-line was filmed by both cameras at a frame rate of 30 000 Fps with the exposure set at 33 μs, adjusted due to the amount of light needed to illuminate the specimen.

The rear surfaces of the panels were cleaned, abraded and then painted with a random speckle pattern which was used in the DIC procedure to determine the spatial deformation of the plate. Full details of the specimen preparation procedure are found in Reference [35].

Table 3- Steel panels' configurations and load parameters- I_{sim} is the impulse from Uncoupled Eulerian analysis, compared against the impulse from experiment by [1]**.**

Configurations			m	$I_{expt.}$	$I_{sim.}$	h_e	Configurations			m	$I_{expt.}$	$I_{sim.}$	h_e
Mat.	S_D **(mm)**	**Model**	**(g)**	**(N.s)**	**(N.s)**	**(mm)**	**Mat.**	S_D **(mm)**	**Model**	**(g)**	**(N.s)**	**(N.s)**	**(mm)**
Mild Steel	25	MS-P1	25	56.4	51.0	3.53	**AMX 370T**	38	AS-P5	40	80.5	78.1	12.72
		MS-P6	40	82.9	82.4	12.72			AS-P6	50	100.1	98.3	15.91
		MS-P8	33	68.2	65.0	10.50			AS-P7	40	82.2	67.1	19.88
		MS-P10	40	80.7	81	12.72			AS-P8	50	91	85.5	24.85
AMX 370T	25	AS-P1	40	80.0	80.1	12.72	**AMX 440T**	25	B3	33	57.3	57.4	10.50
		AS-P2	33	66.1	62.2	10.50			B6	50	94.8	86.0	15.91
	50	AS-P3	40	82.2	78.7	12.72			AX24	24	43.75	43.4	7.31
		AS-P4	70	143.2	135.6	22.27		38	B4	33	57.8	55.0	10.49
									B7	70	129.1	108.2	10.50

4 Methodology of Numerical studies

The numerical simulations were performed in the ABAQUS 6.13® Finite Element hydrocode. The program allows varying degrees of complexity in dealing with the dynamic response of structures subject to blast loads.

The plates were designated shell element type S4(R) with hourglass control. The Numerical models are replicas of the experiments described herein and also those reported by Langdon et al [1]. All the models were fit with two upper and lower clamps along the periphery of the plate were designed as rigid body elements, with a penalty contact and co-efficient of friction of 0.3 between the plate surface and each clamp. An additional width of 20mm on each side of the plate was included for the contact surface with the clamps. Due to symmetry, only a quarter of the plate was modelled.

Three types of numerical simulations were performed: (i) a full 3D Eulerian method, to register the pressure time history and thus obtain the impulse, (ii) a fully coupled Eulerian Lagrangian analysis and (iii) for the sake of comparison, in which a simple pressure-time Lagrangian analysis was performed for MSP8, B3 and ASP2 (with identical charge radius, height and stand-off) having a rectangular pulse load, and load shape localised to the burn area as per Eq.(11) in section 5.4. The magnitude of the load was obtained from the experiment impulse and a 20μs duration for the load was assumed.

4.1 Eulerian methods

In the cases where the empirical approaches fail to conveniently predict the blast response of a material, the use of continuum mechanics algorithms to design the models through the fluid advection and interaction with structure seems necessary. These algorithms are embedded in the Arbitrary Lagrangian-Eulerian (ALE) method, which accounts for obtaining solutions for the arbitrary motion of mesh points with respect to the reference Eulerian points that are fixed in space. In other words, the ALE equations are defined with regards to the material time derivative and reference configuration time derivative [36], [37], and includes Uncoupled and

Coupled Eulerian Lagrangian techniques. The eulerian methods developed here use ALE formulation and fluid structure interaction contact interface, and consist of Coupled and Uncoupled Eulerian lagrangian analyses.

In Uncoupled Eulerian Lagrangian (UEL) models, the multi-materials in the Eulerian medium consisted only of the explosive and air. Rigid boundary conditions were assigned to the Eulerian boundary to monitor the inflow of pressure load shown in Fig. 8, while non-reflecting flow-out boundary conditions were assigned to the side faces along the open fluid boundaries. The register of the pressure time history can be extrapolated and averaged to obtain the mean impulse , as per Equation. (4), and applied in a separate Lagrangian analysis:

$$I = 2\pi \int_0^{\tau} \int_0^{R} r.P(r,t)drdt \tag{4}$$

where I is the impulse imparted to the plate and $P(r,t) = p(r)p(t)$ is the product of load shape and pulse shape parameters. In the numerical model, the mean impulse is compiled by truncating the products of the average impulse density (impulse per unit area) of each element by the area of those elements. A discussion on the transmitted impulse in the UEL models with/without the clamps is presented in section 5.3.1.

There are three distinct phases gauged by the FSI (based on a UEL study of an explosive with $D_e = 50mm$ and $S_D = 38mm$):

1) Phase "i" the expansion of explosive, from time of detonation to its interaction with the structure, denoted t^*, found as $\approx 15\mu s$
2) Phase "ii" explosive plate interaction, which lasts for $36\mu s$.
3) Phase "iii" expansion of the explosion from time of separation from plate to expansion of the plate equilibrium.

The Coupled Eulerian Lagrangian (CEL) accounts for the above three stages as well, but on the deformable structure surface. The CEL technique is based on full coupling of the fluid mesh

points governed by the Eulerian formulations, with the structure mesh points defined by the lagrangian formulations at the fluid structure interface. Detonation was assumed to occur instantanuously. Upon contact with the detonation front, the material point within the unreacted explosive instantanuously transfers to gaseous material which is accompanied with sudden release of energy from the chemical reaction [38], resulting in advection of the gaseous fluid through the mesh points. Advection of the fluid mesh points in the Eulerian medium can be of first or second order. By default, ABAQUS programme burn incorporates second order advection to transfer the state variables (pressure, velocity and explosive product density). This advection method incorporates a process referred to as the flux limiting to ensure the advection is monotonic and to reduce the oscillations occuring after the shock wave. The reader is referred to Reference [39], [40] for further information. Once the fluid reaches the target surface, the FSI is enforced by contact pairs between the fluid mesh points and the structure, allowing the plate to flows throuhg the Eulerian mesh by computing its Eulerian volume fraction within each element. The contact at the fluid structure interface is assumed as frictionless.

A quarter symmetry of the Eulerian cube medium is modelled with a square plan of 300mm with height of 200mm, which encompasses the steel plate with clamps, air medium and the explosive materials (Table 4). The air is modelled with the 'ideal gas' equation of state given in Equation. (5).

Table 4- Explosive and air parameters for Eulerian models

Material	ρ (kg.m^{-3})	Det. Wave speed v (m/s)	A	B	R_1	R_2	ω	E_m	Pre-det. bulk modulus
PE-4	1601	8193	6.0977×10^{11}	1.295×10^{10}	4.5	1.4	0.25	6.057×10^{6}	0
Air	**ρ (kg.m^{-3})**	**$C_p - C_v$ Specific heat constant (Jkg^{-1}K)**		**P (Pa)**	**E_0**	**μ_0 dynamic viscosity ($\mu Pa.s$)**			
	1.293	287		101325	2.5×10^{-4}	18.27			

$$P = (C_p - C_v)\rho_a T \quad \textbf{(5)}$$

where C_p and C_v are the specific heat at constant pressure and volume, respectively, ρ_a is the air density, T is the temperature and P is the pressure. For the air blast explosions, the explosive cylinder is modelled using the Jones-Wilkins Lee equation of state shown in Equation (6).

$$P = A\left(1 - \frac{\omega\rho}{R_1\rho_0}\right)e^{-R_1\frac{\rho_0}{\rho}} + B\left(1 - \frac{\omega\rho}{R_2\rho_0}\right)e^{-R_2\frac{\rho_0}{\rho}} + \frac{\omega\rho^2}{\rho_0}E_{m0} \quad \textbf{(6)}$$

where ρ is the density, ρ_0 density at the beginning of process, A, B, R_1, R_2, and ω are the material constants [38]. The expansion of the explosive is dependent on its geometry. A cylinder of explosive expands primarily in its axial direction rather the radial direction.

For simplicity in obtaining the impulse, the target surface was subdivided into mesh grid zones of 9 elements with the corresponding average pressure. The integral of the pressure load in each zone yields the impulse density value. To obtain the impulse from impulse density, it was assumed that the distribution of the pressure load is axisymmetric over the Cartesian directions. Thus, the integral of the impulse density along the diagonals evaluates the impulse.

5 Results

5.1 Mesh sensitivity and strain localisation

In our initial treatment of each numerical method, we considered a mesh convergence parametric study for the pure Lagrangian and Eulerian Lagrangian methods. The convergence check was set up with three levels of mesh discretisation, from coarse (10×10) to fine (40×40) meshes of S4(R) shell elements. The most suitable mesh was then validated against the experimental models.

In view of the Coupled Eulerian Lagrangian models, the convergence of the plate response as well as the level of impulse were both dependent upon the mesh sizes of the Eulerian medium and the Lagrangian structure whereupon the blast was imparted. The Eulerian medium was discretized with rectangular mesh elements varying from 1.25mm to 10mm (Table 5). The cubic medium was discretised with hexahedral elements which was advantageous over the spherical medium mesh in overcoming the material leakage problems when FSI was involved

[41], [42]. Therefore, the fraction of the medium which accounts for the explosive material contains approximately 40 elements, in accordance with minimum explosive element numbers discussed by [38], [41]. Although such refinement would lead to expensive computations for Eulerian analyses, a finer mesh with infinitesimal time increments may lead the computations to be prone to failure and the coarser mesh would not satisfy the convergence.

Table 5 Element configuration model B4 and AX24

Model config. (AX24 and B4)	no. of elements	Element length (mm)
Steel plates	100	20
	400	10
	1600	5
Eulerian Domain	49392	5-10
	111925	2.5-10
	369820	1.25-10

Table 6 Mesh refinement & $\bar{\varepsilon}_{pl}$of Model B4-AX24

Model config.	Element length/ thickness	W (mm)	$\bar{\varepsilon}_{pl}$
B4	4.33	18.23	1.71
	2.16	25.7	5.42
	1.08	28.2	7.90
AX24	4.33	22.36	2.70
	2.16	24.22	5.40
	1.08	24.4	6.50

Table 6 presents the effect of element refinement on plate deflection and the equivalent plastic strains $\bar{\varepsilon}_{pl}$ taken at time 0.35ms (when principal stresses were maximum). The panels were strained plastically with the onset of loading phase, coupled with strain localisations at the boundaries. Very coarse Lagrangian mesh resulted in simulation errors, which is postulated to be due to excessive relative distortion of the localised elements to their adjacent elements. With the refinement of element length to thickness ratio of ~1, convergence is obtained for the displacements. It is noted that the mesh refinement led to an increase in maximum central deflection, plastic strain and stresses, however, only the deflections were convergent with each

successive refinement. In general, according to [43] the stresses and strains should be convergent if:

$$|\sigma_m - \sigma_c| > |\sigma_f - \sigma_m| \quad (7)$$

with the subscripts denoting the mesh level, viz. σ_c the stress of the coarse mesh, σ_m and σ_f those of the medium and fines meshes, respectively. Yuan and Tan [44] reported that in the convergence study of fully clamped plates, the plastic strain as well as key stresses at the plate boundary ($\bar{\varepsilon}_{pl}$ and σ_{yy}) do not converge with mesh refinement due to stress singularities. Unrealistic strain localisation at the boundaries cannot be deterministic for the ductile fracture modes but has no effect on the study of Mode I (large inelastic deformation) here.

Further investigation of CEL model of the B4 panel (fine mesh) showed that the highest strain was attributed to the localised elements around the middle of boundaries. The plasticity propagated along the support edges and was associated with highest strains at the centre, as well as at the clamp boundaries. The central node experienced an abrupt rise of principal plastic strain (ε_{11}) at 0.08ms, after which the strain rate vanished. Boundary elements, however, underwent a more gradual increase in principal strain (ε_{11}) as the equivalent plastic strain ($\bar{\varepsilon}_{pl}$) approached the plastic strain in the centre, as shown in Fig. 9.

(a) (b)

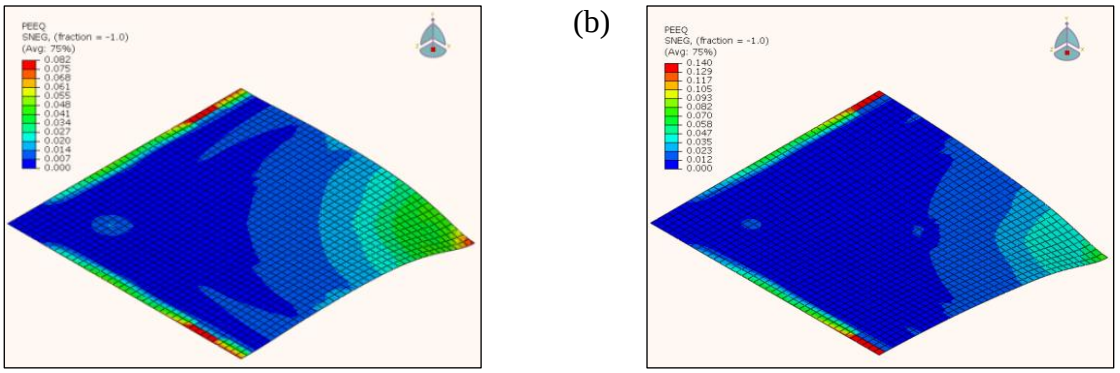

Fig. 9- (a) Equivalent plastic strain @1.167ms (b) Final deformation @3ms. The plastic strain develops inward from the localised boundaries along the plastic hinge lines (For interpretation of colour in this figure, the reader is referred to the online version)..

5.2 Validation of Numerical results

The validity of the numerical studies is assessed by comparing a transient deformation of the ARMOX440T (B4 and AX24) CEL models against the practical values obtained through DIC tests shown in Fig. 10 - Fig. 11. The validation was then investigated on a mild steel panel (denoted MS24 hereinafter) as well as two Armour 500T panels, represented in Fig. 12 and Fig. 13. The load parameters for MS24 comprised of 24g charge mass, 50mm diameter and $S_D = 38mm$. The armour 500T panels were subject to 24g and 33g charge masses and identical configurations to other panels with the exception that H=4.16mm, $\sigma_0 = 1470$ MPa and $S_D = 38mm$. The material properties used for armour 500T were taken from [45]. The specimen B4 was subjected to the impulse of 57.8 N.s, which did not result in rupture of the steel plate.

During the DIC tests, the frame rate of the camera was limited to 30,000fps. This restriction caused motion blur as the plate velocity was high in the initial frames, between 3.2ms-4.0ms shown in Fig. 10. The motion blur resulted in the detail of the central portion of the plate being lost as the speckle pattern could not be resolved.

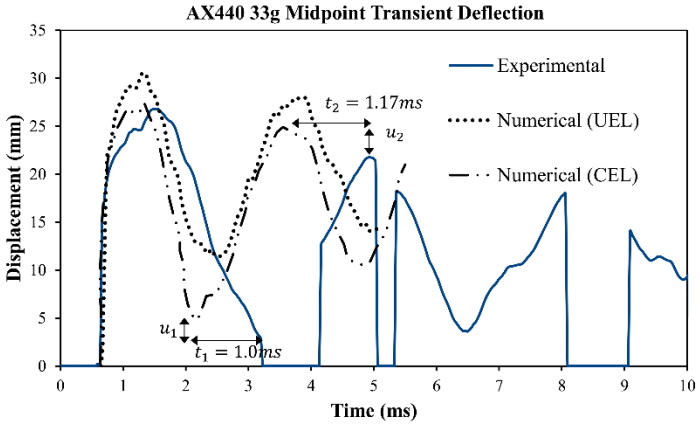

Fig. 10- Time History plot of midpoint displacement, Experiment (from DIC) vs CEL and UEL models, for ARMOX B4.

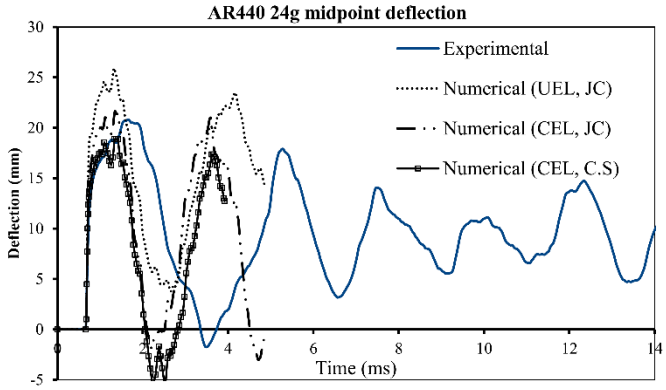

Fig. 11 Time history plots of midpoint displacement, Experiments (from DIC) compared with the CEL and UEL simulations for AX24, based on Cowper Symonds and JC models.

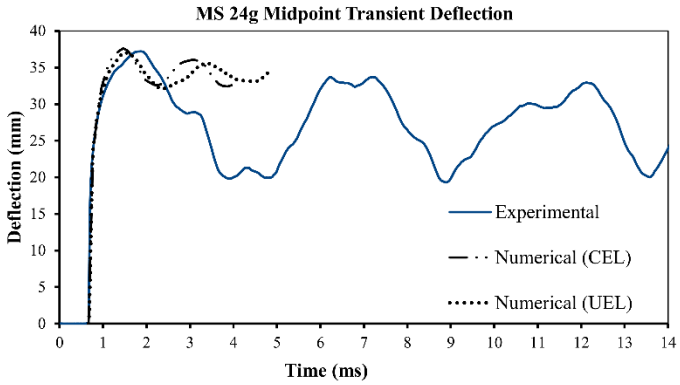

Fig. 12 Time history plots of midpoint displacement, Experiments (from DIC) compared with the CEL.

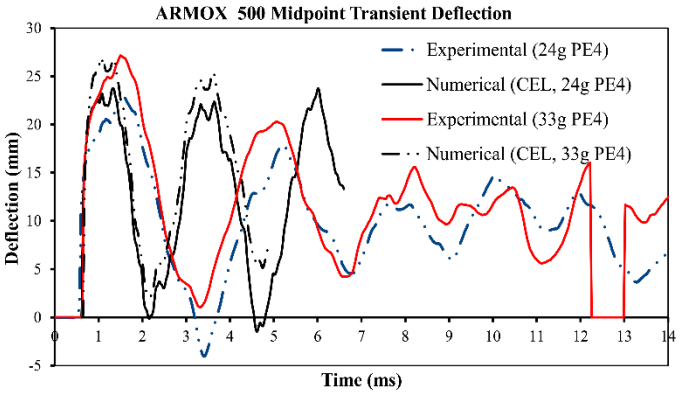

Fig. 13 Time history plots of midpoint displacement, DIC compared with the ARMOX 500T CEL simulations on 33g and 24g PE4 @ 38mm stand-off (For interpretation of colour in this figure, the reader is referred to the online version).

5.3 Comparison of numerical and experimental results

5.3.1 Pressure and impulse

By comparing the displacement and impulse in Table 3, there is a good agreement of total impulse from experiments and the mean calculated impulse from Eulerian simulations, with error of less than 10%.

Following Bonorchis & Nurick [38], a comparison of the pressure time histories from a UEL model with no clamps and one clamp boundary conditions (as is the case of the experimental test) is sought to investigate the influence of boundary conditions on the total impulse transmitted to the plate. The loading arrangements in this comparative study consisted of 40g PE4 explosive, had 50mm diameter and positioned at 50mm stand-off from the target. The UEL model with one clamped was identical to no-clamp case except with specifying rigid chamfers at the edge of the plate, as illustrated in Fig. 14.

Clearly, as shown in Fig. 15, the recorded pressures at gauge points of the two models are coincident and the boundaries have infinitesimal contribution in absorbing the impulse. This is because in the current work, the distance from the plate centre to the boundary was 200 mm, or 2.5 to 5 times the charge diameters (40-75mm) used. Even accounting for the larger stand offs (25-50 mm) used herein, this is considered conservative in preventing the pressure recirculation along the clamp edge observed by Bonorchis and Nurick (2009) at closer boundary distances.

The pressure recirculation in the clamps lasts only for a brief time because the majority of the load has already been dissipated in the plate. The total impulse calculated from the one clamp model was found less than 1.6% higher than the model with no clamp. Thus, the UEL models herein predict the transmitted impulse with reasonable degree of accuracy and compare favourably with the total impulse measured by the ballistic pendulum. As the charge radius to

plate length increases to one third, (as in the case of the model in Ref. [38]) the pressure recirculation duration at the boundaries increase, leading to an increase in the impulse.

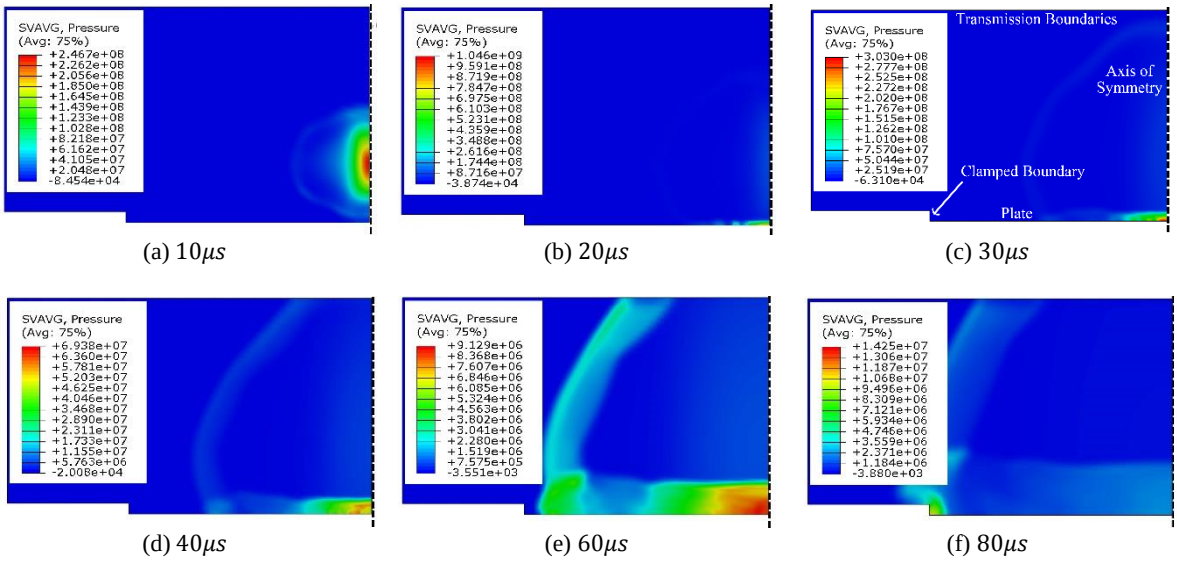

(a) $10\mu s$ (b) $20\mu s$ (c) $30\mu s$

(d) $40\mu s$ (e) $60\mu s$ (f) $80\mu s$

Fig. 14- Distribution of the pressure load at various time points, in the front face of the UEL model with one clamp (For interpretation of colour in this figure, the reader is referred to the online version).

Notably, when the pressure time history is uncoupled from the response (that is, implemented on the structure in a separate simulation) the results are less accurate than in the coupled method. This is due to the structural flexibility taking part in reducing the impulse, the magnitude of the deflection is decreased in fully coupled model [27]. This is due to the thin plate ability to acquire instantaneous velocity which relieves the plate from the pressure acting on the surface, resulting in reduction in the transmitted impulse. However, as the plate thickness increases, this reduction is diminished [23]. Reference [24] extended the work of Taylor [23] on uniform incident waves and expressed the reduction in the transmitted impulse in terms of single dimensionless FSI parameter on compressible fluids and various plate thicknesses. The authors showed that the transmitted impulse ratio depended on the plate mass but is impervious to the shock intensity.

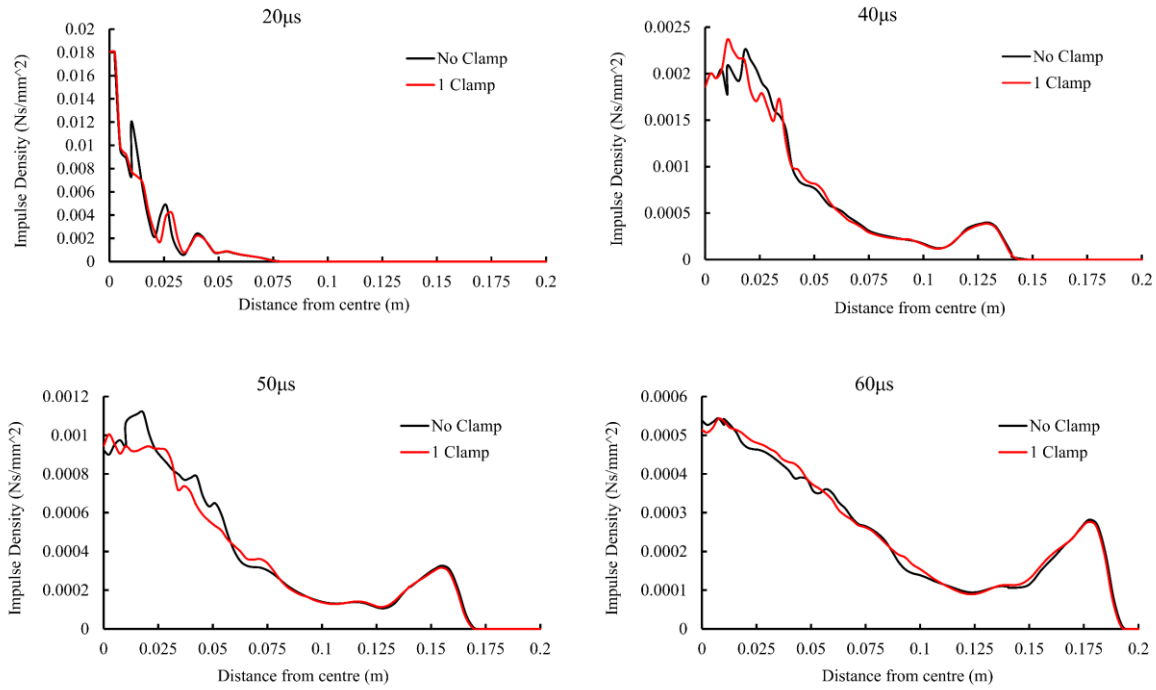

Fig. 15-pressure time histories of 1 clamp compared with no clamp boundary conditions

5.3.2 Deflections and *correlation* of parameters

Table 7 shows the results of the maximum and residual transverse deflections from the numerical and experimental models. It should be mentioned that, while the accuracy of the fully coupled Eulerian analysis is computationally expensive, the CEL analyses registers the outcome with reasonable degree of accuracy, with the similar time history plot of the transverse deflections.

Table 7- Maximum and final deflection of the Steel plates -values in mm.

Material.	Model	w_f. CEL	w_f. Exp.	Variation of W_f CEL from Expt. (%)
Mild Steel	MS-P1	32.25	30.20	6.79
	MS-P6	51.03	53.70	4.97
	MS-P8	47.20	42.00	12.38
	MS-P10	55.50	41.60	33.41
ARMX 370T	ASP1	30.37	29.50	2.95
	ASP2	28.53	21.90	30.27
	ASP3	18.23	14.40	26.60

	ASP4	30.00	25.60	17.19
	ASP5	22.79	21.30	7.00
	ASP6	23.42	27.10	13.58
	ASP7	13.60	17.60	22.73
	ASP8	20.00	18.60	7.53
ARMX 440T	B3	21.78	17.20	26.63
	B4	16.10	14.57	10.50
	B6	16.35	22.10	26.02
	B7	24.50	22.80	7.46

As observed in the Fig. 10- Fig. 13, the predicted vibration by the CEL model lags the actual vibration observed from the experiments. The first minima difference in Fig. 10, $u_1 = 1.96mm$ close to the next peak difference $u_2 = 2.3mm$, and lagging time is maintained throughout, i.e. $t_1 \cong t_2$. It should be mentioned that, the actual prediction of the response is intrinsically difficult as many parameters, including the material rate sensitivity, could affect the transient deformation of the plate as follows. Due to the proximity of the charge, the deformations are localised in narrow shear zones, the response in the central region is governed by the plastic flow in the central region of the plate. The adiabatic heat generated due to the high strain rates gives rise to elevated temperature in the localised region, while the surrounding region strain hardens. This leads adiabatic shear localisation when the thermal softening overcomes the strain hardening effects. [46]

However, for the design purposes, estimating the maximum transverse displacement is usually considered more important than captured the exact nature of the elastic vibrations which follow. The maximum transient displacement may even be preferred over the permanent deformations, since it is the maximum transverse displacement that leads to other types of failure within the panel (such as tensile tearing). Finally, while the relative motion of the frames could give rise to the difference in post peak behaviour, there are many parameters which influence the localised response of the panel - this renders the prediction of transient permanent

deformation intrinsically difficult, and to date few studies are available only on transient deformations experimentally and numerically such as that of Ref. [21], performed on structures subject to uniform blasts.

It is also of interest to study the influence of structural flexibility on the magnitude of the pressure load in the UEL and the fully coupled analysis (CEL). A model with rigid target surfaces was implemented and the recorded pressures at the gauge points on the rigid target surfaces was captured. The predicted pressure-time histories were averaged and implemented in a second stage model with Lagrangian elements. This was an uncoupled model (UEL). The trajectory of transient deformation for the AX24 and MS24 test plates modelled this way are shown in Fig. 10 and Fig. 11. The magnitude of the deformation showed that, using the UEL simulations, averaging the pressure registered on the rigid target surface leads to an increase in the magnitude of maximum deformation. For the various models investigated, the plate maximum deflection obtained from fully coupled analysis was found to be lower than the uncoupled method (Table 8), and closer to the experimental results, with maximum percentage error of 19.7% (UEL) compared to 8.8% (CEL) for the AX24 test. The lower displacement predictions of the CEL occurs as the impulse is diminished by the structural flexibility of the fully coupled model. In other words, for the flexible structure the pressure load obtained from UEL method is an overestimate of the actual pressure load applied to the plate.

Table 8- Maximum mid-point deflection (mm) for Armour and Mild steel

Configuration	AX24	B4	MS24
CEL	19.11	27.20	37.04
UEL	25.91	30.56	33.88
Experiment	20.80	26.78	37.19

The transient deflection profiles of the Armox 440 and Mild Steel models are also compared with those obtained from the DIC tests. The profile shapes of the maximum deflection,

predicted from CEL models, are shown in Fig. 16 and Fig. 17. In Fig. 17a, the transient deformation at maximum peaks 1.08ms and 1.33ms is also compared. The profile shape is similar to the experiment, with more bulging near the boundaries. Further, assuming the same detonation time, it is interesting to note the plate deflection time history responses in Eulerian Lagrangian studies are relatively coincident with the DIC data in maximum and permanent deflections. Despite the affinity, some disparities in the post peak behaviour was observed, with higher spring-back of DIC models (Fig. 12).

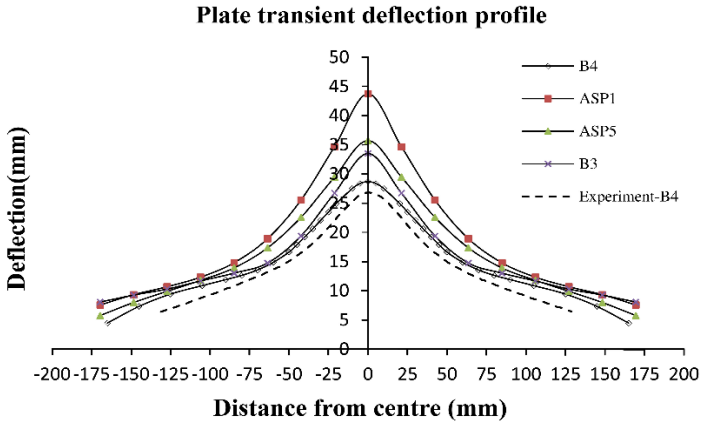

Fig. 16 –Maximum transient deflection profiles –CEL (B4, ASP1, ASP5 and B3) vs experiment(B4)

(a)

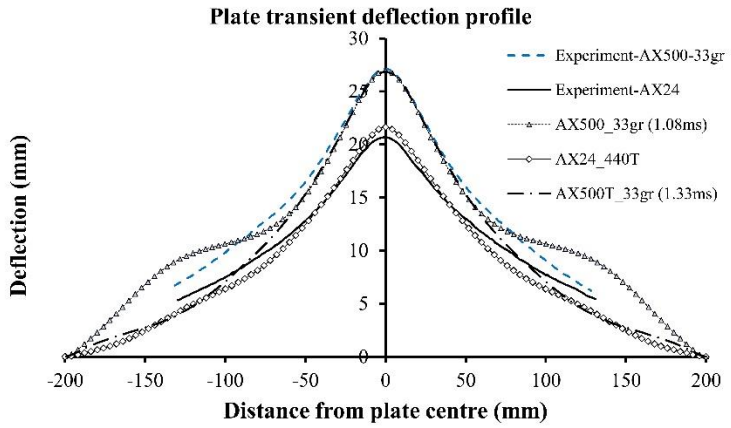

(b)

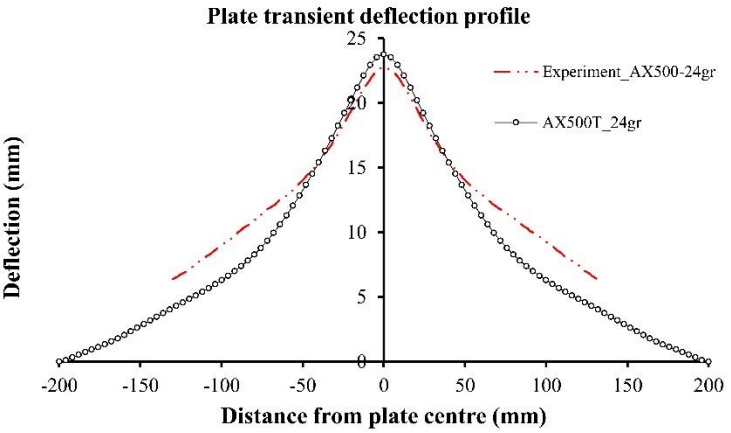

Fig. 17- maximum transient deflection profile of (a) AX500T,33g and AX24 (b) AX500T,24g-CEL vs Experiments

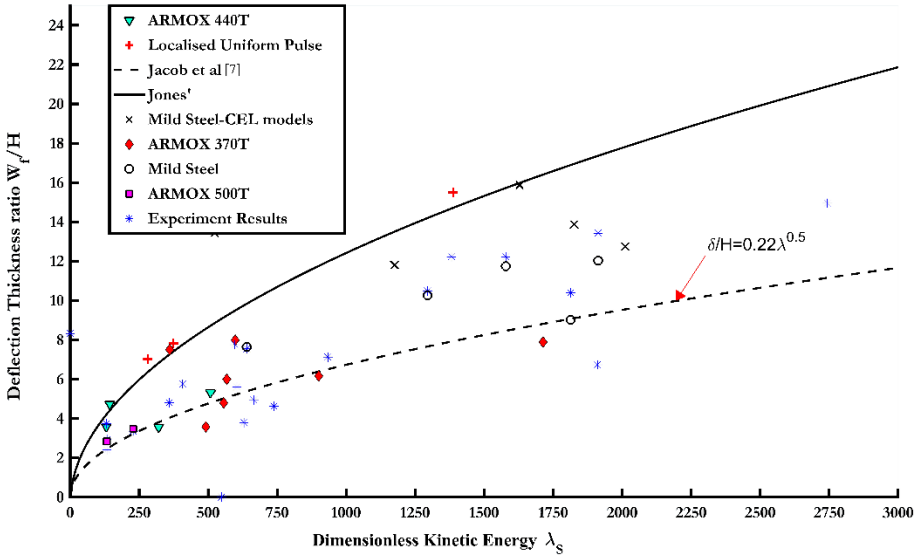

Fig. 18- Comparison of numerical, experimental and empirical results proposed in the literature in dimensionless form.

5.4 Correlation between parameters via empirical studies

Non-dimensional analysis was performed to investigate the difference between the theoretical models, the available empirical models in the literature, and three simulations which ascribe the rigid plastic model subject to the locally uniform pulse.

Experimental and numerical investigations on the effect of load parameters have been calibrated through non-dimensional analysis in the literature. Fundamental theoretical work by Jones [29] has evaluated the plate response to uniform or impulsive loading. The dimensionless kinetic energy, defined by Jones, predicts the large inelastic deformation of the plate loaded impulsively by uniform velocity V_0 as:

$$\lambda = \frac{\mu {V_0}^2 L^2}{M_0 H} \quad \textbf{(8)}$$

In which $M_0 = \frac{\sigma_0 H^2}{4}$is the maximum bending moment per unit length of plate element. The normalised deflection is described by a function of dimensionless kinetic energy λ for quadrangular plates (Equ.(9)).

$$\frac{w_f}{H} = \frac{(1 + \frac{2\lambda}{3})^{0.5} - 1}{2} \quad \textbf{(9)}$$

The uniform velocity of the blast phenomenon is related to the impulse as $I^* = \frac{\hat{I}}{h\sqrt{\sigma_0 \rho}} = \frac{V_0}{\sqrt{\sigma_0/\rho}}$, where $\hat{I}$ and I^* are the impulse density and dimensionless impulse [44]. The authors of [44] report that, most blast loads are, in fact, non-impulsive and the validity of such idealisation depends on the blast duration being shorter than the structural response time.

For a plate loaded impulsively by localised blast, Equ. (8) is replaced by empirical Equ.(10), where A_0 is the burn area. The burn area of the plate is defined by the phenomenon where explosive particles discolour the central plate. The burn radius R_b, according to [8] can be empirically obtained via Equ. (11), where h_e is the charge height. Jones' [29] dimensionless

kinetic energy can be related to the dimensionless impulse ϕ_{ql}. The relationship between the normalised deflection and ϕ_{ql} has been empirically addressed by [7], [16] and [38].

$$\lambda_1 = \frac{4I^2L^2}{\rho\sigma_0 {A_0}^2 H^4} \quad \textbf{(10)}$$

$$\frac{R_b}{r_e} = 0.9h_e^{0.3} \quad \textbf{(11)}$$

$$\emptyset_{ql} = \frac{I\left(1 + \ln(\frac{LB}{\pi {r_e}^2}\right)}{2H^2(LB\rho\sigma_0)^{1/2}} \quad \textbf{(12)}$$

$$\frac{w_f}{H} = 0.48\emptyset_{ql} \quad \textbf{(13)}$$

$$\frac{w_f}{H} = 0.47\emptyset_{ql} + 0.001 \quad \textbf{(14)}$$

Jacob et al [16] reported from [34] a damage number for quadrangular plates as $\lambda_1 = 4\beta {\phi_q}^2$, hence obtained the Equ. (12), by adding $(1 + \ln\left(\frac{LB}{\pi {r_e}^2}\right))$ to account for load idealisation, where $\beta = L/B$. With normalising the impulse, named damage number hereunder, the permanent deflection can be obtained through empirical Equ. (13) and (14) by Nurick and Martin [10], [34], thus, the new dimensionless kinetic energy is $\lambda_S = 4\beta {\phi_{ql}}^2$.

The results from various models, including a pure Lagrangian analysis with rectangular pulse shape (determined from impulse and uniform load shape over central region) for ASP2, MSP8 and B3 panels, were cast in dimensionless form and presented in Fig. 18. The numerical results are compared against Jones' [29] theoretical predictions, and are similar to the pure Lagrangian model. However, Jones' theoretical predictions overestimate the plate response in the localised blast load for the other models and the experiments. Hence, in the idealisation of the blast load, the temporal variation of the load plays a significant role and Jones' idealisation is similar to the Lagrangian models in assuming an impulsive load. The actual load is to be considered as dynamic rather than purely impulsive [27]. For example, consider the load parameters $m_e =$

$33gr$, $S_D = 38mm$ and $D_e = 50mm$, which has the exponential positive pulse duration $\tau = 30\mu s$, giving the region affected by the blast-taken as the position of the plate inflexion point in the plate profile- 60mm away from the midpoint. Evaluating the natural frequency $(\omega)$of the plate by a modal analysis, we calculated the abscissa of pressure impulse diagrams [47], $\omega\tau = 0.5$, sufficiently high to regard the load as dynamic. Similar results would ensue with decreasing the charge mass. However, when the stand-off distance decreased to 25mm, the pressure load increases, causing larger transverse deformation. Consequently, the position of the inflexion point would increase to 80mm, suggesting rather impulsive load type with $\omega\tau = 0.26$. A transition from the idealised, partially impulsively loaded panels to the actual load shape, which is exponentially varying across the panel, leads to a significant difference between the simple models and the CEL approach.

It should also be mentioned that; the material mesh elements can be idealised as rigid when the ratio of kinetic energy to the maximum strain energy stored elastically is sufficiently high to virtually ignore the influence of material elasticity. This condition is can be applied to mild steel material model, for which the idealisation of pulse shape as per Equ. (9) will not render much disparity in terms of accuracy. However, ignoring material elasticity of high strength steel in the theoretical analyses will lead to inaccurate predictions.

It transpires that the results are bounded between the Jones' model and the empirical trends found from experiments of References [7], [10]. Equ. (14) was employed by Langdon et al [1] to investigate the relationship between the impulse and the final plate deflection for armour steel. However, the effect of stand-off distance was ignored. The relationship of the normalised impulse was later altered by Jacob et al [7], to make the comparison of blast-loaded panels of different geometries and characteristic stresses, to take an account of the loading parameters. The authors introduced a scaling coefficient to parameterise the stand-off distance, which is accounted for in the cases where $s_D > r_e$ as per Equ. (15), (16).

$$\gamma'_s = \frac{\left(1+\ln\left(\frac{LB}{\pi r_e^2}\right)\right)}{\left(1+\ln\left(\frac{S_D}{r_e}\right)\right)} \quad \textbf{(15)}$$

$$\emptyset_{sq'} = \frac{I\gamma'_s}{2H^2\sqrt{(LB\rho\sigma_0)}} \quad \textbf{(16)}$$

Through the regression analysis, the final-normalised-displacement of the plate can be circumscribed to the Equ. (18) with the ± 1 bounds. The plot of the results, which account for the stand-off distance is shown in Fig. 19.

Fallah et al [48] reported that a fit to the experiments was achieved by using the slenderness ratio, defined in Equ. (17), into empirical Equ. (16) to yield Equ. (19):

$$\gamma_{sl} = \left(\frac{H}{B}\right)^m \quad \textbf{(17)}$$

$$\frac{w_f}{H} = 0.52\emptyset_{sq'} + 1.1 \quad \textbf{(18)}$$

$$\emptyset_{sl} = \emptyset_{sq'}\gamma_{sl} = \frac{I\gamma'_s\gamma_{sl}}{2H^2\sqrt{(LB\rho\sigma_0)}} \quad \textbf{(19)}$$

$$\emptyset_{sl'} = \frac{I\gamma'_s}{2B^2\sqrt{(L\mu\sigma_0)}} \quad \textbf{(20)}$$

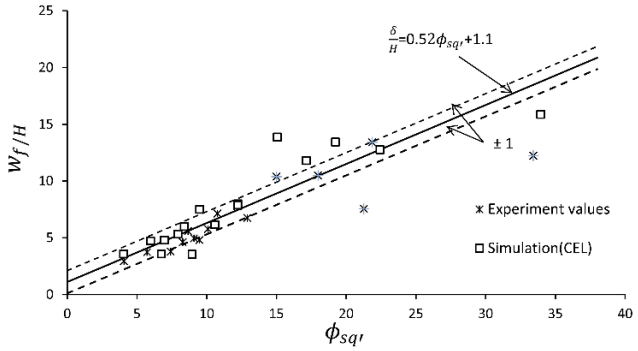

Fig. 19- Damage number $\emptyset_{sq'}$ vs the normalised displacement

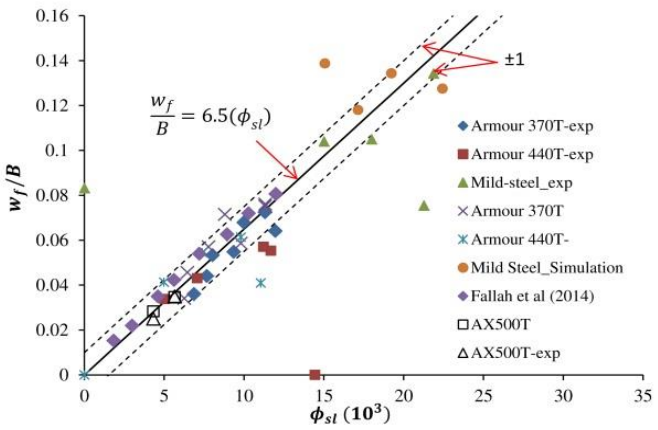

Fig. 20- Correlations of permanent deflection/width ratio with the damage parameter $\emptyset_{sl}$

The normalised displacement is related to the equation of best fit, the parameter 'm' from Equ. (17) accounts for the material type, which was found to be 1.6 for Dyneema® HB26 panels and armour steel panels [48]. Assuming $m = 1.5$, Equ. (19) can further be simplified to Equ. (20) without loss of accuracy in the regression line, as illustrated in the Fig. 20.

It is also noted that, the experimental models by [1] (outlined in Table 3) exhibited the mode I failure and did not rupture. Previous experimental research, according to [1], showed that both mild steel and Armox steel plates ruptured for identical laod parameters ($S_D = 25mm$, $m = 40g$ and $D_e = 50$. This leads to the feasibility of establishing the rupture impulse that was not solely based on the strength of the steel. The non-dimensional analysis performed herein shows that these models attain the highest dimensionless impulses, $\emptyset_{sq'} = 12.22$ and 22.42, for armour steel 370T and mild steel, respectively. Clearly, even though the model ASP4 undergoes highest impulse (143N.s), it does not rupture as the higher stand-off/charge diameter ratio contributes toward reduction of the normalised impulse [49]. Therefore, These parameters of $\emptyset_{sq'}$ can be used for the preliminary design applications, to obtain the panel geometry (such as the desired thickness), based on simple algebraic manupulations from the Equ. (20), when the strain rate sensitivity of the material is ignored. Details of the preliminary design is presented by reference [48].

However, Reference [1] suggests that while the rupture impulse is partially influenced by the material ductility, other failure mechanisms such as specific energy to tensile failure (SETF), which is a measure of both strength and ductility of the material, contribute to the rupture behaviour. Since the SETF is known a priori (it is obtained from the quasi static tensile test), it is a useful indicatoor of rupture behaviour of different material types [1].

The design procedure can be carried out in the following manner: based on the load parameters and using Equ. (4), the average impulse that a blast threat can generate is measured empirically. Hence the non-dimensional analysis is performed to predict whether the steel panel (Armox steel or Mild steel) exceeds this value of rupture impulse and to pinpoint the final deformation of the panel. Clearly, the complex nature of the loading and the materials strain rate sensitivity make it difficult to generalise the empirical values for all Armour steel and mild steel panels, but these values can be used as 'safe' design parameters together with consideration of SETF.

5.4.1 Distribution of blast Load

The localised blast load has a spatial (load shape) and temporal (pulse shape) variation. In most works of the literature [38], [50], [51] the load shape is assumed to be constant over the central region and decay exponentially in a radial direction outside this zone, as illustrated in Equ. (21).

In Fig. 21 the spatial variation of registered pressure from the Eulerian analysis across the plate breadth was validated using the linear regression analysis. In most cases the percentage error of 5% was noticed, which indicates a good fit of the data points with exponential pressure equation with coefficient of confidence R^2 >90% , as presented in Table 9.

The temporal variation is influenced by the pulse shape. According to [50], [52], the final deformation of a non-impulsive loaded plate is strongly dependent on the pulse shape; however, using the correlation parameters of Reference [52]-effective pressure, mean time and

effective impulse- the pulse shape efects can be eliminated. A comparison of pressure time history for mild steel and armour steel Eulerian models is made in Fig. 22 at 23mm away from the plate centre. In Fig. 22-a the effect of charge mass is evident, however by comparison of deflections in Table 8 and pressure in Fig. 22-b it can be deduced that the model B4 has dissipated more energy than MS24 in spite of the same pressure (impulse).

$$\begin{cases} \mathrm{p(r)} = \mathrm{p_0} & 0 \le r \le r_e \\ \mathrm{p(r)} = \mathrm{ap_0 e^{-br}} & r_e \le r \le r_{plate} \end{cases} \quad (21)$$

Table 9- load parameters of explosive

Config.	Explosive parameters ap_0e^{-br}		R^2
	ap_0 (GPa)	Decay constant, b	
ASP1	3.11	104.13	97.30%
ASP7	2.14	101.25	90.04%
B4	2.85	96	91.95%
ASP4	3.054	69.04	95.69%

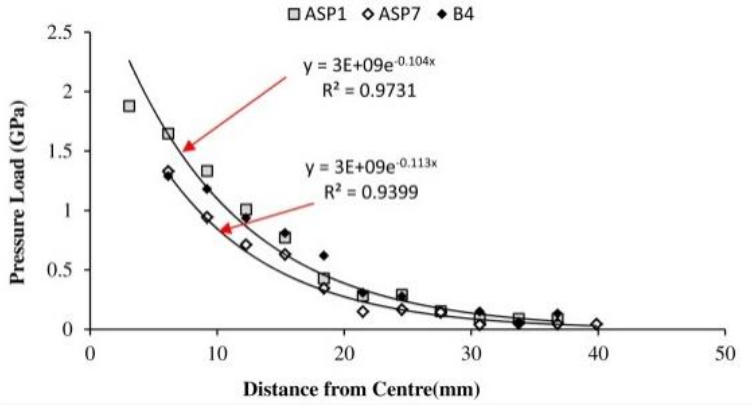

Fig. 21– Curve fitting of the pressure load based on regression

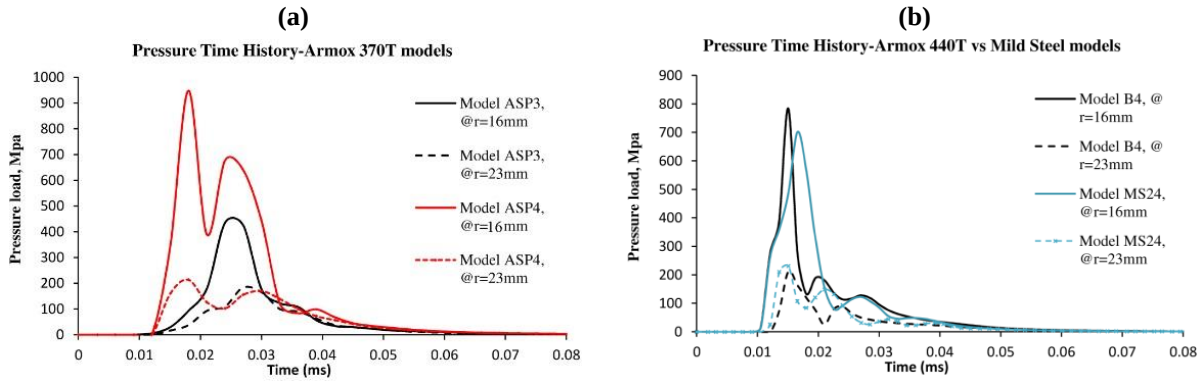

Fig. 22- Pressure time history of steel plates (a) ARMOX 370T- (b) B4 vs MS24

6 Conclusions

An experimental and numerical study on the response of armour steel to localised air-blast loading is reported herein. The experimental data supplemented the data set presented in reference [1] with additional blast test results and was used validate the various numerical techniques. The numerical methods consisted of a coupled and an uncoupled Eulerian Lagrangian analysis. Dimensionless analysis and the theoretical models by [29] were used to evaluate the results.

Regarding the CEL analysis, closer correlations in impulses from the blast waves were observed. The regression analysis also showed good fit of the monitored pressure load along the plastic hinge lines to Equ. (21). Hence both Eulerian Lagrangian methods, viz., UEL and CEL, predicted more accurate response of the steel plates, although the coupled method exhibited a closer correlation with the actual behaviour of the plates. For the coupled model, the FSI governs the performance of the plate. Clearly, the plate mass and stiffness influence the FSI effect. Increase in the thickness would affect both the mass and the stiffness of the plates. For example, an increase of the plate thickness from 3.81mm to 4.61mm increases the ratio of the transmitted impulse to total impulse on rigid target by average of 3%. Since the plates considered here are relatively thin ($0.95\% < H/L < 1.1\%$), the transmitted impulse is reduced due to the FSI effects, which justifies the lower deformation in CEL analysis compared to the UEL analysis. In the UEL analysis, the plate stiffness approaches infinity, all the incident pressure is reflected off the surface and full impulse is imparted to the plate

As expected, the ARMOX steel panels exhibited lower maximum and residual plastic deformations due to the higher ability of energy dissipation from the blast, which subsequently increase as the material yield strength increases (ARMOX 550T compared to 370T or mild steel).

The CEL models results closely correlated with those of the experiments regarding both maximum and final plate deflection. The theoretical model by Jones [29] considerably overestimates the armour steel plate midpoint deflection, in which the pulse shape and the material elasticity are the more impact factors than the material strain rate sensitivity. Henceforth, prediction of the deformation based on idealisation of uniform pulse for localised blast load would yield inaccurate results.

7 References

[1] G. S. Langdon, W. C. Lee, and L. A. Louca, "The influence of material type on the response of plates to air-blast loading," *Int. J. Impact Eng.*, vol. 78, pp. 150–160, 2015.

[2] M. Y. Yahya, W. J. Cantwell, G. S. Langdon, and G. N. Nurick, "The Blast Behavior of Fiber Reinforced Thermoplastic Laminates," *J. Compos. Mater.*, vol. 42, no. 21, pp. 2275–2297, 2008.

[3] A. Chen, L. A. Louca, and A. Y. Elghazouli, "Blast assessment of steel switch boxes under detonation loading scenarios," *Int. J. Impact Eng.*, vol. 78, pp. 51–63, 2015.

[4] S. B. Menkes and H. J. Opat, "Broken beams - Tearing and shear failures in explosively loaded clamped beams," *Exp. Mech.*, vol. 13, no. 11, pp. 480–486, 1973.

[5] G. N. Nurick and A. M. Radford, "Deformation and tearing of clamped circular plates subjected to localised central blast loads," *Recent Dev. Comput. Appl. Mech. (Ed. B.D Reddy)*, vol. a volume i, pp. 276–301, 1997.

[6] M. D. Olson, G. N. Nurick, and J. R. Fagnan, "Deformation and rupture of blast loaded square plates—predictions and experiments," *Int. J. Impact Eng.*, vol. 13, no. 2, pp. 279–291, 1993.

[7] N. Jacob, G. N. Nurick, and G. S. Langdon, "The effect of stand-off distance on the failure of fully clamped circular mild steel plates subjected to blast loads," *Eng. Struct.*, vol. 29, no. 10, pp. 2723–2736, 2007.

[8] S. Chung Kim Yuen and G. N. Nurick, "The significance of the thickness of a plate when subjected to localised blast loads," *Blast Impact Load. Struct.*, pp. 471–499, 2000.

[9] R. G. Teeling-Smith and G. N. Nurick, "The deformation and tearing of thin circular plates subjected to impulsive loads," *Int. J. Impact Eng.*, vol. 11, no. 1, pp. 77–91, 1991.

[10] G. N. Nurick and J. B. Martin, "Deformation of thin plates subjected to impulsive loading - A review - Part II - Experimental results," *Int. J. Impact Eng.*, vol. 8, no. 2, pp. 171–186, 1989.

[11] V. H. Balden and G. N. Nurick, "Numerical simulation of the post-failure motion of steel plates subjected to blast loading," *Int. J. Impact Eng.*, vol. 32, no. 1–4, pp. 14–34, 2006.

[12] T. Wierzbicki and G. N. Nurick, "Large deformation of thin plates under localised impulsive loading," *Int. j. Impact Engng*, vol. 18, no. 96, pp. 899–918, 1996.

[13] G. N. Nurick and V. . Balden, "Localised Blast Loaded Circular Plates: an Experimental and Numerical Investigation," *Proc. IMPLAST 2010 Conf.*, vol. 12, no. 14, pp. 145–152, 2010.

[14] G. N. Nurick, M. D. Olson, J. R. Fagnan, and a. Levin, "Deformation and tearing of blast-loaded stiffened square plates," *Int. J. Impact Eng.*, vol. 16, no. 2, pp. 273–291, 1995.

[15] G. N. Nurick, M. E. Gelman, and N. S. Marshall, "Tearing of blast loaded plates with clamped boundary conditions," *Int. J. Impact Eng.*, vol. 18, no. 7–8, pp. 803–827, 1996.

[16] N. Jacob, S. C. K. Yuen, G. N. Nurick, D. Bonorchis, S. A. Desai, and D. Tait, "Scaling aspects of quadrangular plates subjected to localised blast loads - Experiments and predictions," *Int. J. Impact Eng.*, vol. 30, no. 8–9, pp. 1179–1208, 2004.

[17] A. Neuberger, S. Peles, and D. Rittel, "Springback of circular clamped armor steel plates subjected to spherical air-blast loading," *Int. J. Impact Eng.*, vol. 36, no. 1, pp. 53–60, 2009.

[18] A. Neuberger, S. Peles, and D. Rittel, "Scaling the response of circular plates subjected to large and close-range spherical explosions. Part II: Buried charges," *Int. J. Impact Eng.*, vol. 34, no. 5, pp. 874–882, 2007.

[19] W. L. Fourney, U. Leiste, R. Bonenberger, and D. J. Goodings, "Mechanism of loading on plates due to explosive detonation," *Fragblast*, vol. 9, no. 4, pp. 205–217, 2005.

[20] K. Spranghers, I. Vasilakos, D. Lecompte, H. Sol, and J. Vantomme, "Identification of the plastic behavior of aluminum plates under free air explosions using inverse methods and full-field measurements," *Int. J. Solids Struct.*, vol. 51, no. 1, pp. 210–226, 2014.

[21] V. Aune, E. Fagerholt, K. O. Hauge, M. Langseth, and T. Børvik, "Experimental study on the response of thin aluminium and steel plates subjected to airblast loading," *Int. J. Impact Eng.*, vol. 90, pp. 106–121, 2016.

[22] V. Aune, G. Valsamos, F. Casadei, M. Larcher, M. Langseth, and T. Børvik, "Numerical study on the structural response of blast-loaded thin aluminium and steel plates," *Int. J. Impact Eng.*, vol. 99, pp. 131–144, 2017.

[23] G. I. Taylor, "The pressure and Impulse of Submarine Explosion Waves on Plates," *The Scientific Papers of Sir Geoffrey Ingram Taylor*, vol. III, no. 4. Cambridge University Press, Cambridge, UK, pp. 287–303, 1963.

[24] N. Kambouchev, R. Radovitzky, and L. Noels, "Fluid–Structure Interaction Effects in the Dynamic Response of Free-Standing Plates to Uniform Shock Loading," *J. Appl. Mech.*, vol. 74, no. 5, p. 1042, 2007.

[25] N. Kambouchev, L. Noels, and R. Radovitzky, "Nonlinear compressibility effects in fluid-structure interaction and their implications on the air-blast loading of structures," *J. Appl. Phys.*, vol. 100, no. 6, 2006.

[26] W. Grobbelaar and G. Nurick, "An investigation of Struvctures Subjected to Blast Loads Incorporating an Equation of State to Model the Material Behaviour of the Explosives," in *7th International Symposium on Structural Failure and Plasticity (IMPLAST*

2000), 2000, pp. 185–194.
[27] T. Børvik, A. G. Hanssen, M. Langseth, and L. Olovsson, “Response of structures to planar blast loads - A finite element engineering approach,” *Comput. Struct.*, vol. 87, no. 9–10, pp. 507–520, 2009.
[28] S. Chung Kim Yuen, G. S. Langdon, G. N. Nurick, E. G. Pickering, and V. H. Balden, “Response of V-shape plates to localised blast load: Experiments and numerical simulation,” *Int. J. Impact Eng.*, vol. 46, pp. 97–109, 2012.
[29] N. Jones, *Structural Impact*, 1st ed. Cambridge: Cambridge University Press, 1997.
[30] N. Jones, “Dynamic inelastic response of strain rate sensitive ductile plates due to large impact, dynamic pressure and explosive loadings,” *Int. J. Impact Eng.*, vol. 74, pp. 3–15, 2013.
[31] G. R. Johnson and W. H. Cook, “Fracture characteristics of three metals subjected to various strains, strain rates, temperatures and pressures,” *Eng. Fract. Mech.*, vol. 21, no. 1, pp. 31–48, 1985.
[32] K. Vedantam, D. Bajaj, N. S. Brar, and S. Hill, “Johnson - Cook strength models for mild and DP 590 steels,” *AIP Conf. Proc.*, vol. 845 I, no. 2006, pp. 775–778, 2006.
[33] SSAB, “Armox 440T Blast protection plate,” 2017. [Online]. Available: http://www.ssab.co.uk/products/brands/armox/armox-440t.
[34] G. N. Nurick and J. B. Martin, “Deformation of thin plates subjected to impulsive loading-a review -Part I: Theoretical considerations,” *Int. J. Impact Eng.*, vol. 8, no. 2, pp. 159–170, 1989.
[35] R. J. Curry and G. S. Langdon, “Transient response of steel plates subjected to close proximity explosive detonations in air,” *Int. J. Impact Eng.*, vol. 102, pp. 102–116, 2017.
[36] M. Souli, A. Ouahsine, and L. Lewin, “ALE formulation for fluid-structure interaction problems,” *Comput. Methods Appl. Mech. Eng.*, vol. 190, no. 5–7, pp. 659–675, 2000.
[37] R. van Loon, P. D. Anderson, F. N. van de Vosse, and S. J. Sherwin, “Comparison of various fluid-structure interaction methods for deformable bodies,” *Comput. Struct.*, vol. 85, no. 11–14, pp. 833–843, 2007.
[38] D. Bonorchis and G. N. Nurick, “The influence of boundary conditions on the loading of rectangular plates subjected to localised blast loading - Importance in numerical simulations,” *Int. J. Impact Eng.*, vol. 36, no. 1, pp. 40–52, 2009.
[39] Simulia, “ABAQUS Analysis user’s Manual,” *Cambridge University*. 2017.
[40] M. Larcher and F. Casadei, “Explosions in Complex Geometries - A Comparison of Several Approaches,” *Int. J. Prot. Struct.*, vol. 1, no. 2, pp. 169–195, 2010.
[41] J. Trajkovski, R. Kunc, J. Perenda, and I. Prebil, “Minimum mesh design criteria for blast wave development and structural response-MMALE method,” *Lat. Am. J. Solids Struct.*, vol. 11, no. 11, pp. 1999–2017, 2014.
[42] S. H. Tan, J. K. Poon, R. Chan, and D. Chng, “Retrofitting of Reinforced Concrete Beam-Column via Steel Jackets against Close-in Detonation,” in *12th International LS-Dyna Users Conference*, 2012, no. 3, pp. 1–12.
[43] G. B. Sinclair, J. R. Beisheim, and S. Sezer, “Practical convergence-divergence checks for stresses from FEA,” *Proc. 2006 Int. ANSYS Conf.*, vol. 50, no. Reference 1, 2006.
[44] Y. Yuan and P. J. Tan, “Deformation and failure of rectangular plates subjected to impulsive loadings,” *Int. J. Impact Eng.*, vol. 59, pp. 46–59, 2013.
[45] P. Skoglund, M. Nilsson, and A. Tjernberg, “Fracture modelling of a high performance armour steel,” *J. Phys. IV Fr.*, vol. 134, pp. 197–202, 2006.
[46] T. Børvik, O. S. Hopperstad, T. Berstad, and M. Langseth, “A computational model of viscoplasticity and ductile damage for impact and penetration,” *Eur. J. Mech. A/Solids*, vol. 20, no. 5, pp. 685–712, 2001.
[47] W. E. Baker, P. A. Cox, P. S. Westine, J. J. Kulesz, and R. A. Strehlow, *Explosion Hazards and Evaluation*. Amsterdam-Oxford-New York: ELSEVIER Scientific Publication Company, 1983.
[48] A. S. Fallah, K. Micallef, G. S. Langdon, W. C. Lee, P. T. Curtis, and L. A. Louca, “Dynamic response of Dyneema® HB26 plates to localised blast loading,” *Int. J. Impact Eng.*, vol. 73, pp. 91–100, 2014.
[49] K. Micallef, A. Soleiman, D. J. Pope, M. Moatamedi, L. A. Louca, and H. Road, “On dimensionless loading parameters for close-in blasts,” *Int. Jounral Multiphysics*, vol. 9, no. 2, pp. 171–194, 2015.
[50] K. Micallef, a. S. Fallah, D. J. Pope, and L. A. Louca, “The dynamic performance of simply-supported rigid-plastic circular steel plates subjected to localised blast loading,” *Int. J. Mech. Sci.*, vol. 65, no. 1, pp. 177–191, 2012.
[51] G. S. Langdon, S. C. K. Yuen, and G. N. Nurick, “Experimental and numerical studies on the response of quadrangular stiffened plates. Part II: Localised blast loading,” *Int. J. Impact Eng.*, vol. 31, no. 1, pp. 85–111, 2005.
[52] C. K. Youngdahl, “Influence of pulse shape on the final plastic deformation of a circular plate,” *Int. J. Solids Struct.*, vol. 7, no. 9, pp. 1127–1142, 1971.